PIER Letters

(Received 23 July 2024, Accepted 19 September 2024, Scheduled 14 October 2024)

Magnetic Resonance Eddy Current Detection for Rebar Corrosion in Concrete

Xiaoming She[1], Haitao Chen[2], Zhengxuan Zhang[2], Jinming Zhang[2], and Leng Liao[2, *]

[1] *CCCC First Highway Consultants Co., Ltd., Xi'an 710075, China*
[2] *School of Materials Science and Engineering, Chongqing Jiaotong University, Chongqing 400074, China*

ABSTRACT: Rebar corrosion is a common hidden danger in concrete structures, posing a serious threat to structural safety. Due to its concealed nature, detecting rebar corrosion remains a significant challenge. Recently, a new detecting principle for internal rebar corrosion: Magnetic Resonance Eddy Current Penetration Imaging (MREPI) is proposed. This method significantly enhances the detection depth of eddy currents through resonance amplification. In this work, the theoretical and numerical analysis of MREPI has been done. The results demonstrate the higher sensitivity than the traditional eddy current testing (ECT). Furthermore, we built an MREPI sensor by using nanocrystalline soft magnetic metal as magnetic core to detect the rebar corrosion, Experimental results show that the proposed sensor can effectively test rebar within concrete, with the imaging patterns of corroded rebar being distinguishable.

1. INTRODUCTION

Reinforced concrete structures leverage the strengths of both rebar and concrete, making them highly prevalent in construction engineering [1]. However, environmental factors and the chemical properties of the materials can cause rebar to corrode when it is exposed to air and moisture over time. This corrosion diminishes the cross-sectional area of the rebar, potentially leading to structural failure. Therefore, developing effective methods for detecting and imaging rebar corrosion in reinforced concrete structures is of significant, practical, and application value.

Current nondestructive testing technologies, such as electrochemical methods [2], acoustic emission [3], and magnetic flux leakage [4], can detect rebar corrosion but fail to accurately identify internal structural damage. Consequently, researchers have been working to develop imaging technologies capable of detecting internal structures, such as ultrasonic scanning imaging [5] and infrared thermal imaging [6]. However, due to the large size and complexity of reinforced concrete structures, these conventional imaging methods have limitations in meeting the on-site requirements for rebar corrosion detection.

The eddy current testing (ECT) can not only achieve the imaging of reinforcement corrosion detecting, but also quantify the corrosion detecting. As a non-destructive testing method, Koido and Hoshikawa (1995) utilized artificial neural network technology in eddy current testing to study the thickness of the rebar protective layer and rebar diameter [7]. De Alcantara et al. [8] combined finite element methods with experiments using ECT technology to investigate rebar corrosion in reinforced concrete, finding a strong linear relationship between the degree of corrosion and the analysis characterization parameters. When imaging rebar corrosion is inside concrete, it is necessary to combine eddy current heating with infrared detection, which complicates the detection process. Additionally, the imaging results are influenced by the moisture content of the concrete and structural complexity. Therefore, traditional ECT technology faces challenges in achieving the precise imaging of internal rebar corrosion.

In recent years, significant breakthroughs have been made in the field of foreign object detection using magnetic resonance wireless power transmission systems. Kurs et al. [9] proposed a magnetic coupling resonance wireless power transmission technology based on strong coupled electromagnetic resonance effects, which significantly improved wireless energy transmission efficiency. Liu and Dong [10, 11] enhanced the displacement detection system of a transmitting-receiving dual-coils through magnetic resonance, effectively increasing the sensing distance compared to traditional eddy current sensors. Hor et al. [12] explored the impact of the relative positions of ferrite cores and coils, as well as components like capacitors and resistors, on the sensitivity of the detection system using electromagnetic simulation based on resonance eddy current detection technology. Hughes et al. [13] employed near-resonance technology to observe and characterize previously unrecorded small defects in titanium 6-4. Zhang et al. [14] integrated magnetic resonance into magneto-elastic inductance method, analyzing the correlation between stress and induced voltage, and found that magnetic resonance enhancement effectively improved the accuracy of stress detection. Chen et al. [15] built a magnetic resonance eddy current penetration imaging system by using ferrite as core and successfully get the image of rebar corrosion in concrete.

In this study, a simulation has been done by finite element method, and the results demonstrate that the sensitivity of this sensor is markedly improved compared to traditional eddy cur-

* Corresponding author: Leng Liao (lengliao@cqjtu.edu.cn).

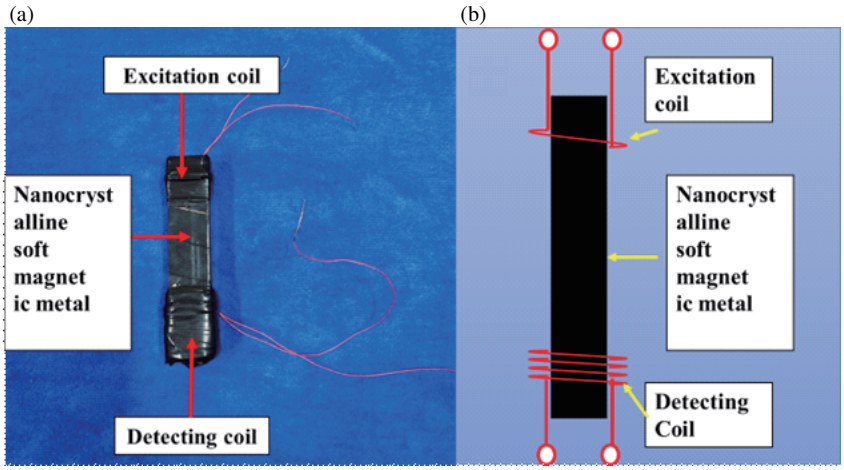

FIGURE 1. (a) The MREPI sensor; (b) The physical model of the MREPI sensor.

rent testing (ECT). Different from the previous work, we built MREPI sensor by using nanocrystalline soft magnetic metal to detect the rebar corrosion. Experimental results show that the proposed magnetic resonance eddy current sensor can effectively image rebar within concrete, with the imaging patterns of corroded rebar being distinguishable. These findings introduce a new approach for the nondestructive imaging of rebar corrosion in concrete structures.

2. THEORETICAL ANALYSES

Based on magnetic coupling resonance technology, we propose a sensor as shown in Figure 1. The excitation coil and detection coil are coaxially wound on nanocrystals, which concentrate the magnetic flux at the center of each coil.

The magnetic resonance eddy current sensor employs a dual-coil structure with separate detection and excitation coils. Due to the typically higher number of turns in the detection coil, its parasitic capacitance must be considered. The equivalent circuit of the magnetic resonance eddy current sensor is shown in Figure 2, where the metal specimen is modeled as an LR circuit, consisting of a series connection of resistor R_3 and inductor L_3.

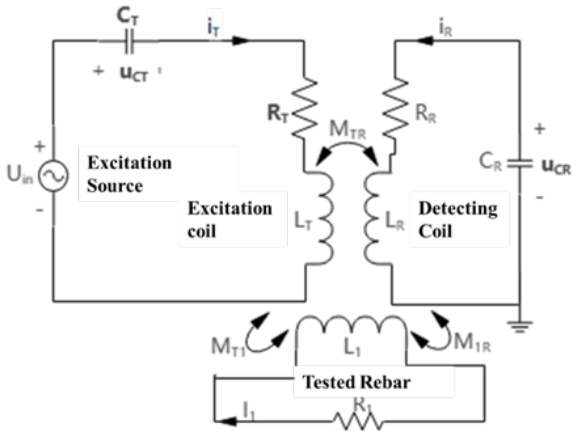

FIGURE 2. Equivalent circuit diagram of the dual-coil sensor detection model.

According to coupled mode theory [15], the general coupled mode equations for the LC circuit system [17] can be expressed as equations:

$$\frac{da_{\pm}(t)}{dt} = (\pm j\omega_m - \Gamma_m)\, a_{m\pm}(t) \pm \sum_{n\neq m} jK_{mn}a_{n\pm}(t) + F_m(t) \quad (1)$$

where j represents the imaginary unit, and $a_{m\pm}$ is referred to as the modal amplitude, indicating the complex conjugate of the energy storage in the m-th LC circuit. ω_m is the resonant angular frequency of the m-th LC circuit, Γ_m the loss rate, $F_m(t)$ is the driving source, and K_{mn} the influence and energy relationship between the m-th and n-th LC circuits. To simplify the analysis, the complex conjugates $a_{m\pm}$ can be represented using either the positive or negative form, ignoring the subscripts for positive and negative forms.

Incorporating magnetic resonance technology, the dual-coil sensor separates the detection and excitation phases. When the frequency of the changing magnetic field generated by the excitation coil matches the detection coil, the detection coil resonates. The rebar is modeled as an R_1 circuit, where a resistor R is in series with an inductor L, and U_{in} is the excitation voltage. u_{CT} and u_{CR} represent the voltages across the parasitic capacitances, while i_T and i_R are the currents in the circuit. $L_T(L_R)$ and $C_T(C_R)$ are the inductances and parasitic capacitances of the coils, respectively.

In coupled-mode theory, the energy conversion shown in Figure 2 can be described by Equation (2):

$$\begin{aligned}
\frac{da_T}{dt} &= j\omega_T a_T - \Gamma_T a_T + jK_{TR}a_R + jK_{T1}a_1 + Fe^{j\omega t} \\
\frac{da_R}{dt} &= j\omega_R a_R - \Gamma_R a_R + jK_{RT}a_T + jK_{R1}a_1 \quad (2) \\
\frac{da_1}{dt} &= j\omega_1 a_1 - \Gamma_1 a_1 + jK_{1T}a_T + jK_{1R}a_R
\end{aligned}$$

$$\omega_T = \frac{1}{\sqrt{L_T C_T}} \quad \omega_R = \frac{1}{\sqrt{L_R C_R}} \tag{3}$$

$$\Gamma_T = \frac{R_T}{2L_T} \quad \Gamma_R = \frac{R_R}{2L_R} \quad \Gamma_1 = \frac{R_1}{2L_1} \tag{4}$$

$$K_{TR} = \frac{\omega_0 M_{TR}}{2\sqrt{L_T L_R}} \quad K_{T1} = \frac{\omega_0 M_{T1}}{2\sqrt{L_T L_1}} \quad K_{R1} = \frac{\omega_0 M_{R1}}{2\sqrt{L_R L_1}} \tag{5}$$

Here, a_T, a_R, and a_1 represent the stored energy modal amplitudes of the excitation coil, detection coil, and the object under test, respectively. The angular frequencies ω_T of the excitation coil and ω_R of the detection coil are determined by Equation (3). The loss rates Γ_T, Γ_R for the excitation coil and Γ_1 for the object under test are determined by Equation (4). The coupling coefficients K_{TR}, K_{T1}, and K_{R1} in the model are determined by Equation (5).

The excitation signal is provided by the signal generator $Fe^{j\omega t}$ where F is expressed as in Equation (6); ω is the angular frequency of the excitation signal; u_{in} the effective excitation voltage; U_{in} is the effective value of u_{in}; and $e^{j\omega t}$ is the complex signal equivalent to $cos\,(\omega t) + jsin\,(\omega t)$.

$$F = \frac{U_{in}}{2\sqrt{L_T}} \tag{6}$$

Since K_{TR}=K_{RT}, K_{T1}=K_{1T}, K_{R1}=K_{1R}, the steady-state solution of the system can be derived from Equation (2) as:

$$a_R = \frac{(j\Gamma_1 K_{TR} - jK_{TR}(\omega-\omega_1) - K_{T1}K_{R1})Fe^{j\omega t}}{\begin{bmatrix} \Gamma_T K_{R1}^2 + \Gamma_R K_{T1}^2 + \Gamma_1 K_{TR}^2 + \Gamma_T\Gamma_R\Gamma_1 \\ -\Gamma_T(\omega-\omega_R)(\omega-\omega_1) - \Gamma_R(\omega-\omega_T)(\omega-\omega_1) \\ -\Gamma_1(\omega-\omega_R)(\omega-\omega_T) \end{bmatrix} +}$$

$$j\begin{bmatrix} (-2K_{TR}K_{T1}K_{R1} + \Gamma_T\Gamma_R(\omega-\omega_1) \\ +\Gamma_T\Gamma_1(\omega-\omega_R) + \Gamma_R\Gamma_1(\omega-\omega_T) \\ +K_{TR}^2(\omega-\omega_1) + K_{T1}^2(\omega-\omega_R) + K_{R1}^2(\omega-\omega_T) \\ -(\omega-\omega_T)(\omega-\omega_R)(\omega-\omega_1) \end{bmatrix} \tag{7}$$

According to the definition of energy storage in an LC circuit, the stored energy in the receiving circuit can be expressed as Equation (8), where U is the voltage across the detection coil. When the angular frequency of the excitation signal ω matches the natural frequencies of the excitation coil, detection coil, and the object under test, ω_T=ω_R=ω_1.

$$|a_T|^2 = \frac{1}{2}\left(L_T i_T^2 + C_T u_{CT}^2\right) = \frac{1}{2}C_T U^2 \tag{8}$$

Since the excitation coil is relatively far from the test piece, Γ_{T1}=$\Gamma_{1T}$$\approx 0$. When the operating frequency is sufficiently high, combining Equations (4), (6), and (8), Equation (7) can be simplified to Equation (9);

$$U_R = \frac{j2\sqrt{2L_T}R_1 L_R M_{TR} F e^{j\omega t}}{(M_{R1}^2 R_T + M_{TR}^2 R_1)} \tag{9}$$

In Equation (9), M_{TR} and M_{R1} represent the coupling coefficients between the excitation coil and detection coil, and between the detection coil and the object under test, respectively.

$$i_R = \frac{U_R}{Z_R} = \frac{j\sqrt{2}R_1 M_{TR} U_{in} e^{j\omega t} L_R}{Z_R \omega \sqrt{L_R C_R}(M_{R1}^2 R_T + M_{TR}^2 R_1)} \tag{10}$$

The current i_R in the detection coil can be determined from Equation (9) as given by Equation (10), where $Z_R = R_R + j(\omega L_R - \frac{1}{\omega C_R})$. Traditional eddy current sensors can obtain the current i_R in the detection coil according to the above Equations (1), (2), (3), (4), (5), (6), and (8), resulting in Equation (11):

$$i_R = \frac{\sqrt{2}U_{in}L_1 R_R e^{j\omega t}}{Z_R\sqrt{L_R C_R}\omega^2 M_{R1}^2} \tag{11}$$

In practical measurements, the probe of the proposed magnetic resonance eddy current sensor is manufactured with a fixed distance between the detection coil and excitation coil. Therefore, M_{TR} will be considered as a constant. Since it is difficult to measure the detection voltage of traditional eddy current methods, the currents i_R for the magnetic resonance sensor's detection coil and i_R for the traditional eddy current detection coil are both normalized with respect to the variation of M_{R1}, and then plotted in Figure 3.

In Figure 3, both i_R and i_R decrease as the mutual inductance M_{R1} increases. However, as M_{R1} increases, the rate of decay of i_R is much slower than that of i_R. This implies that the magnetic resonance eddy current sensor has a longer detection distance and higher sensitivity for detecting rebar. As there is a correlation between rebar corrosion imaging and the current in the detection coil, we conducted simulations and experiments for detecting rebar corrosion inside concrete using the sensor.

3. SIMULATION

To better explain the characteristics of the proposed sensor, numerical simulations were conducted by using finite element numerical method. A sinusoidal voltage with an amplitude of 0.5 V was used to excite the excitation coil, with a distance of 8 cm between the excitation coil and detection coil. To obtain a high-quality mesh, each domain was meshed separately using tetrahedral elements. Additional fine meshing was applied to the domains of the excitation coil and detection coil to enhance the sensor's accuracy. The 2D simulation results of the sensor's magnetic field are shown in Figure 4.

As shown in Figure 4(b), the red arrows represent the magnetic field distribution of the sensor. The depth of the red arrows in Figure 4(a) is much weaker than Figure 4(b) because the magnetic field distribution in the non-resonant state has not reached its maximum. The analysis of Figure 4(b) shows that in the resonant state, the magnetic fields of both coils are distributed between the coils and the nanocrystals magnetic core. This implies that the sensor's probe has high sensitivity, consistent with theoretical calculations. Therefore, the magnetic resonance sensor with this structure possesses high sensitivity.

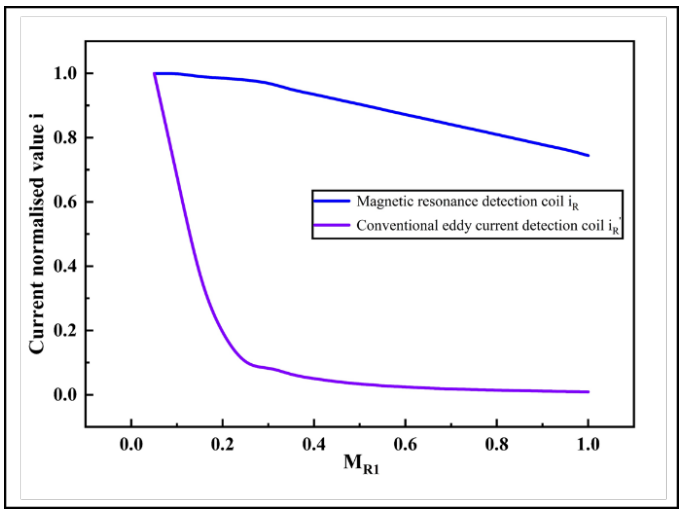

FIGURE 3. Variation of currents i_R and i_R with mutual inductance M_{R1}.

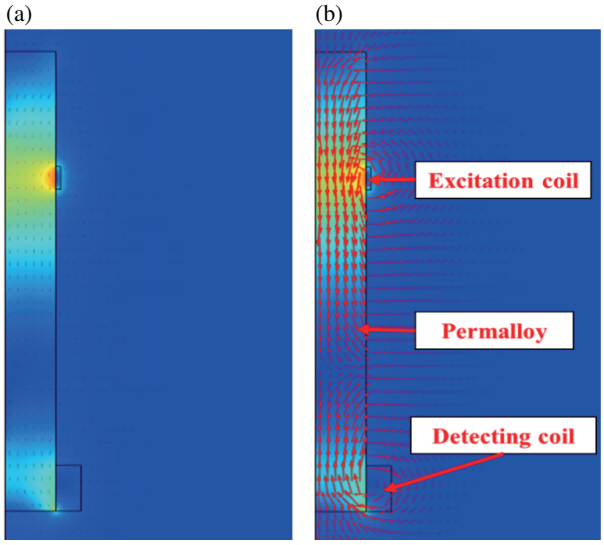

FIGURE 4. 2D sensor simulation of magnetic field distribution: (a) non-resonant state, (b) resonant state.

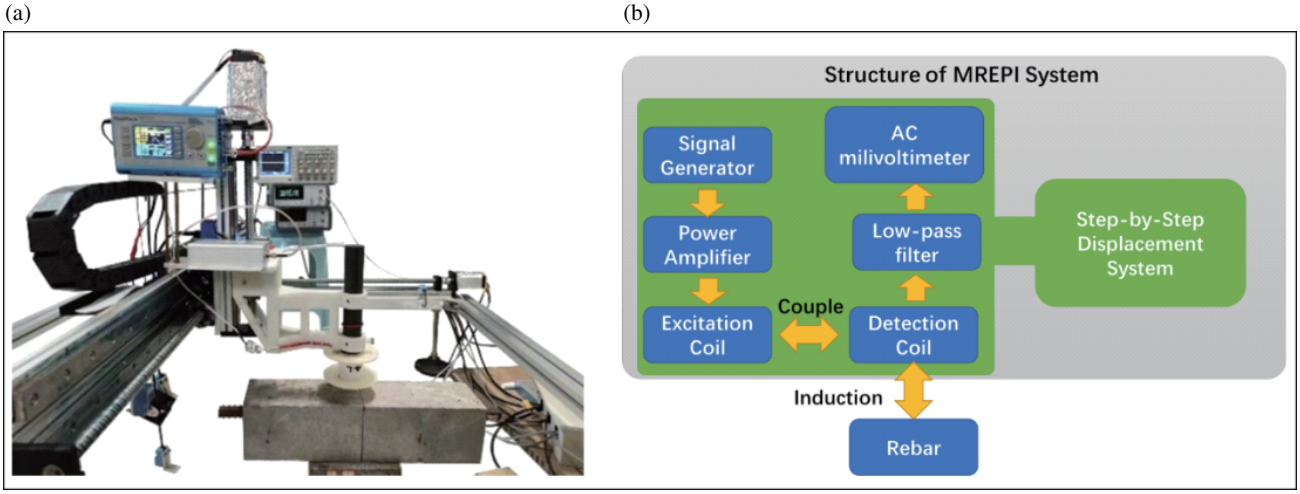

FIGURE 5. MREPI system: (a) The physical MREPI equipment; (b) The structure of MREPI system.

4. EXPERIMENTS

The measurement system developed by our laboratory for rebar concrete scanning imaging is shown in Figure 5. It includes a signal generator, a magnetic resonance eddy current sensor, a filter, a digital AC millivoltmeter, and a computer. The sensor consists of an excitation coil, a detection coil, and a nanocrystals magnetic core. The magnetic resonance eddy current sensor is composed of an excitation coil and a detection coil. The signal generator is connected to an amplifier, which is then connected to the excitation coil to provide a sinusoidal excitation signal with a voltage of 0.5 V. The digital AC millivoltmeter is connected to the filter, which is then connected to the detection coil, and it is used to measure the effective value of the induced voltage.

After installing the sensor, the excitation frequency of the detection system needs to be adjusted so that the peak induced voltage value on the detection coil is maximized, thereby improving the detection range and accuracy. In this experiment, the system achieved the maximum induced voltage in the detection coil at an excitation frequency of 75.6 kHz. Therefore, setting the excitation frequency to 75.6 kHz allows the magnetic resonance eddy current detection system to operate at its optimum.

Under the condition of a 35 mm lift-off height, imaging scans were performed on both a concrete specimen with an 18 mm diameter rebar and a corroded rebar concrete specimen according to the scanning path shown in Figure 6. The peak induced voltages measured from the detection coil, collected by the digital AC voltmeter, were normalized to obtain V_τ. The 2D imaging was then created using V_τ. The imaging results for the rebar concrete and corroded rebar concrete are shown in Figure 6.

Figure 7(a) shows that along the Y direction of the rebar axis, the V_τ values are roughly the same, and the color bands are also

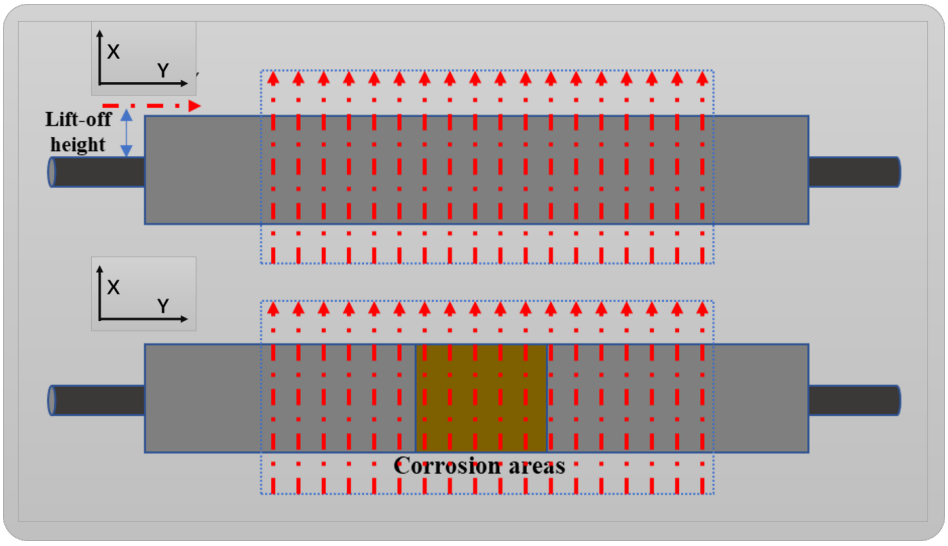

FIGURE 6. Scanning path for rebar concrete imaging.

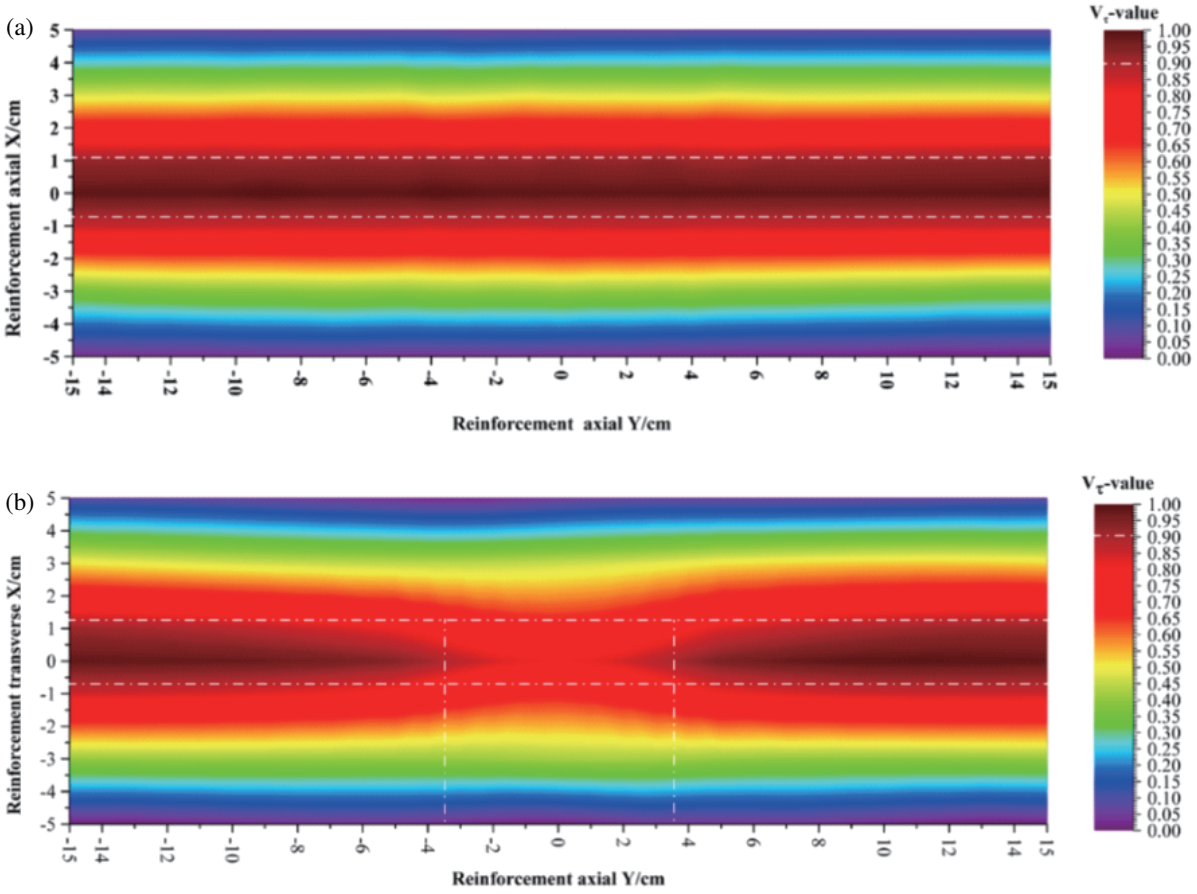

FIGURE 7. Imaging results: (a) Rebar concrete; (b) Corroded rebar concrete.

consistent. The differences along the Y direction of the rebar are due to the uneven placement of the specimen. Along the X direction of the rebar, the V_τ values exhibit significant differences, showing a trend of being smaller at the sides and larger in the middle. In the figure, this is reflected by the deeper color band in the middle and lighter color bands on the sides, with a nearly symmetrical pattern. Corresponding to the imaging results with the scanning path, it is found that the area with the highest V_τ value, where the color band is the deepest, indicates the position of the rebar. Therefore, as the sensor gets closer to the specimen, the signal difference increases. The red and black color bands in the figure represent the direction and location of

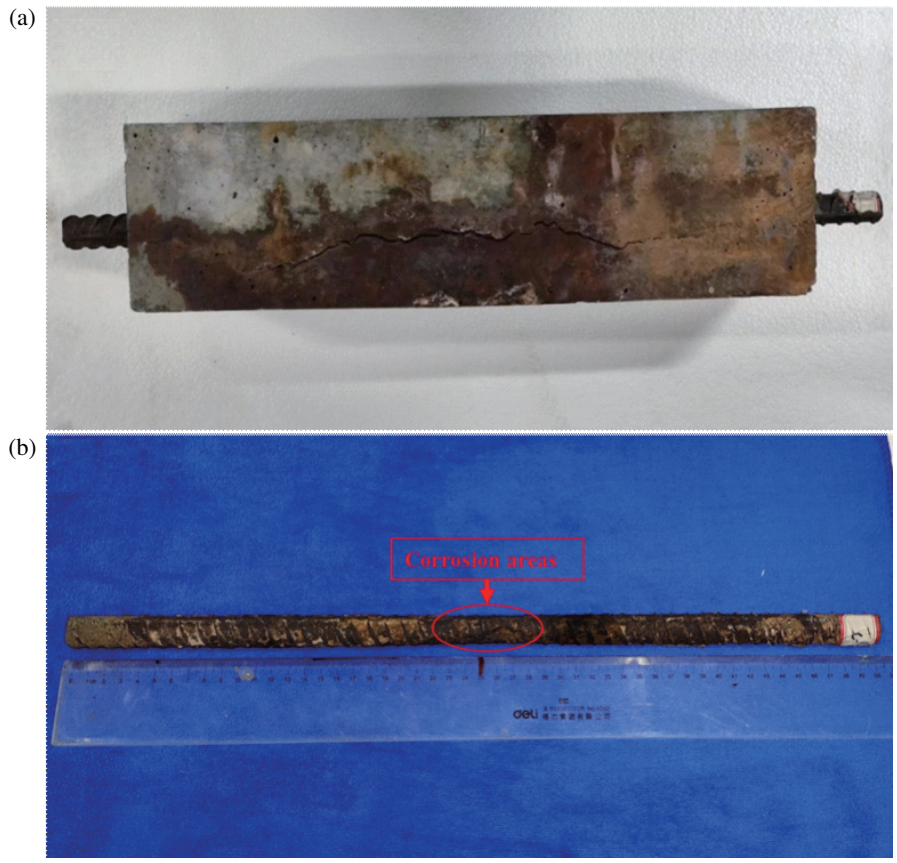

FIGURE 8. Actual results: (a) Corroded reinforced concrete; (b) Corroded rebar within concrete.

the rebar, successfully achieving the imaging and positioning of the rebar within the concrete. In Figure 7(b), after the rebar corrodes, the color band pattern along the X direction still shows a deeper middle and lighter sides, maintaining a nearly symmetrical pattern. The maximum V_τ value along the X direction still appears at the position of the rebar. However, along the Y direction of the rebar, the V_τ values are no longer consistent. In the corroded area, the V_τ values significantly decrease, and the color band becomes lighter. The red and black color bands that were present in the two-dimensional imaging of the intact rebar show breaks in the corroded areas, indicated by the intersections of the white dotted lines in the figure, which correspond to the corroded areas of the rebar.

The actual condition of the reinforced concrete is shown in Figure 8.

In Figure 8(a), the actual corrosion of the reinforcement is depicted, while Figure 8(b) shows the corrosion of the rebar inside the concrete after breaking open the concrete. The corroded areas in the image correspond to the dashed white lines in Figure 7(b), and the widths of the corrosion in the rebar also match. The fuzzy similarity formulations have been used to process the data to make the 2D image obtained by eddy current detection method closer to the real object [18, 19], so our team will improve the imaging accuracy from the data processing aspect later. Therefore, the eddy current sensor using magnetic resonance technology can achieve imaging of the corrosion in the reinforcement within concrete.

5. CONCLUSION

Analysis and simulation both indicate that magnetic resonance technology can effectively enhance the sensitivity and detection distance of traditional eddy current imaging. By using an MREPI sensor built with nanocrystalline soft magnetic metal, the imaging of the corrosion in the reinforcement inside 20 mm protective layer thickness of reinforced concrete has been achieved. The position and orientation of the reinforcement can be clearly determined based on the magnitude of V_τ values, and the corroded areas can also be identified in the two-dimensional image. Therefore, the MREPI method provides a new approach for nondestructive detection of corrosion in steel reinforcement in concrete structures, demonstrating high practical and academic value.

ACKNOWLEDGEMENT

This study was supported by the National Natural Science Foundation of China (52278146), the Natural Science Foundation of Chongqing, China (CSTB2023NSCQ-LZX0062).

REFERENCES

[1] Lu, C., W. Jin, and R. Liu, "Reinforcement corrosion-induced cover cracking and its time prediction for reinforced concrete structures," *Corrosion Science*, Vol. 53, No. 4, 1337–1347, 2011.

[2] Bouchar, M., E. Foy, D. Neff, and P. Dillmann, "The complex corrosion system of a medieval iron rebar from the Bourges' Cathedral. Characterization and reactivity studies," *Corrosion Science*, Vol. 76, 361–372, 2013.

[3] Zhang, J., H. Ma, W. Yan, and Z. Li, "Defect detection and location in switch rails by acoustic emission and Lamb wave analysis: A feasibility study," *Applied Acoustics*, Vol. 105, 67–74, 2016.

[4] Qiu, J., H. Zhang, J. Zhou, H. Ma, and L. Liao, "Experimental analysis of the correlation between bending strength and SMFL of corroded RC beams," *Construction and Building Materials*, Vol. 214, 594–605, 2019.

[5] Miró, M., J. N. Eiras, P. Poveda, M. A. Climent, and J. Ramis, "Detecting cracks due to steel corrosion in reinforced cement mortar using intermodulation generation of ultrasonic waves," *Construction and Building Materials*, Vol. 286, 122915, 2021.

[6] Fang, G., W. Ding, Y. Liu, J. Zhang, F. Xing, and B. Dong, "Identification of corrosion products and 3D distribution in reinforced concrete using X-ray micro computed tomography," *Construction and Building Materials*, Vol. 207, 304–315, 2019.

[7] Koido, J. and H. Hoshikawa, "Covering thickness and diameter measurement of reinforcing bars by eddy current testing using neural network," *Review of Progress in Quantitative Nondestructive Evaluation*, 841–847, 1995.

[8] De Alcantara, N. P., F. M. Da Silva, M. T. Guimarães, and M. D. Pereira, "Corrosion assessment of steel bars used in reinforced concrete structures by means of eddy current testing," *Sensors*, Vol. 16, No. 1, 15, 2016.

[9] Kurs, A., A. Karalis, R. Moffatt, J. D. Joannopoulos, P. Fisher, and M. Soljačić, "Wireless power transfer via strongly coupled magnetic resonances," *Science*, Vol. 317, No. 5834, 83–86, 2007.

[10] Liu, C. and Y. Dong, "Resonant coupling of a passive inductance-capacitance-resistor loop in coil-based sensing systems," *IEEE Sensors Journal*, Vol. 12, No. 12, 3417–3423, 2012.

[11] Liu, C. and Y. Dong, "Resonant enhancement of a passive coil-capacitance loop in eddy current sensing path," *Measurement*, Vol. 45, No. 3, 622–626, 2012.

[12] Hor, Y. L., Y. Zhong, V. P. Bui, and C. E. Png, "Electrical resonance eddy current sensor for submillimeter defect detection," in *Nondestructive Characterization and Monitoring of Advanced Materials, Aerospace, and Civil Infrastructure 2017*, Vol. 10169, 535–541, Portland, Oregon, United States, 2017.

[13] Hughes, R., Y. Fan, and S. Dixon, "Near electrical resonance signal enhancement (NERSE) in eddy-current crack detection," *NDT & E International*, Vol. 66, 82–89, 2014.

[14] Zhang, S., H. Zhang, H. Liu, J. Zhou, C. Yin, and L. Liao, "Resonance enhanced magnetoelastic method with high sensitivity for steel stress measurement," *Measurement*, Vol. 186, 110139, 2021.

[15] Chen, H., L. Liao, J. Zhou, H. Zhang, S. Zhang, T. Lan, Z. Zhang, and C. Hu, "Magnetic resonance eddy penetrating imaging for detecting reinforcement corrosion in concrete," *Automation in Construction*, Vol. 165, 105512, 2024.

[16] Dean, K. J., "Waves and fields in optoelectronics: Prentice-hall series in solid state physical electronics," *Physics Bulletin*, Vol. 35, 339, 1984.

[17] Koh, K. E., T. C. Beh, T. Imura, and Y. Hori, "Impedance matching and power division using impedance inverter for wireless power transfer via magnetic resonant coupling," *IEEE Transactions on Industry Applications*, Vol. 50, No. 3, 2061–2070, 2014.

[18] Versaci, M., G. Angiulli, P. Crucitti, D. De Carlo, F. Laganà, D. Pellicanò, and A. Palumbo, "A fuzzy similarity-based approach to classify numerically simulated and experimentally detected carbon fiber-reinforced polymer plate defects," *Sensors*, Vol. 22, No. 11, 4232, 2022.

[19] Versaci, M., G. Angiulli, P. di Barba, and F. C. Morabito, "Joint use of eddy current imaging and fuzzy similarities to assess the integrity of steel plates," *Open Physics*, Vol. 18, No. 1, 230–240, 2020.